

Performing spin-polarized STM experiments theoretically

P. Weinberger

*Center for Computational Nanoscience, Seilerstätte 10/22, A1010 Vienna, Austria**and Max-Planck-Institut für Mikrostrukturphysik, Weinberg 2, Halle, D06120 Saale, Germany*

(Received 11 November 2009; revised manuscript received 15 January 2010; published 13 May 2010)

By introducing paths on the hypersurface of the band-energy contribution (free energy) to the magnetic anisotropy energy and of corresponding differences in the zz -like elements of the electric conductivity tensor, viewed as an implicit function of the free energy, experimental spin-polarized scanning tunnel microscope (STM) data, namely, the recording of a differential current as a function of an externally applied field, can be analyzed and facilitate a direct comparison between theory and experiment. It is shown that along different paths rather different flipping times of the direction of the magnetization can occur. In particular, discussed are in terms of “theoretical experiments” horizontal and vertical movements of the tip, the influence of the magnetic properties of the tip as well as of typical samples. Furthermore, it is claimed that because of different time scales in a (presently still fictional) time-resolved mode for spin-polarized STM experiments even particular paths on these hypersurfaces could be mapped out.

DOI: [10.1103/PhysRevB.81.174410](https://doi.org/10.1103/PhysRevB.81.174410)

PACS number(s): 75.75.-c, 75.70.-i, 75.47.-m

I. INTRODUCTION

In the last few years the number of publications devoted to spin-polarized scanning tunnel microscopy (STM) increased substantially, see, e.g., Refs. 1–4, claiming that by now even the magnetic switching properties of single atoms or at least of very small islands of magnetic atoms can be determined experimentally. The progress made is indeed impressive since now a days even the use of external surprisingly high magnetic vector fields becomes possible. The lateral precision in moving the tip is already reduced to a fraction of the spatial extension of an atom on top of a surface. Technologically, of course, the ultimate miniaturization of magnetic recording media is sought after, although the physical phenomena per se cause quite a lot of curiosity. The samples usually consist of an ensemble of magnetic atoms placed on a suitable substrate such as, for example, Cu(111) or Pt(111). Very often a so-called Cr/W tip is used of unfortunately little known geometrical structure, the tip itself consisting usually of some ten Cr layers and quite a lot of W layers that in turn are connected to a lead. The width of the vacuum barrier between the sample and the tip is typically below 10 Å.

Although mostly still based on the ideas of Bardeen⁵ and Tersoff and Hamann⁶ theoretical approaches made also a lot of progress, see, e.g., Refs. 7–9, since as compared to the early stage of STM, it was realized that for noncollinear magnetic moments and flipping properties spin-orbit interactions had to be included¹⁰ at least in terms of the so-called second variation method.¹¹ Most recent theoretical studies, dealing with spin-polarized STM in one or the other way, are confined to evaluations of the electronic structure and the magnetic properties of the adsorbates and rely on the Tersoff-Hamann model to offer a sufficiently close mapping of the experimental measurements. In most experiments, however, only a laterally (well) resolved change in the tunneling current is measured as a function of the applied external field, the current being of course a nonlocal quantity that reflects all physical properties of the sample and the tip between

appropriately fixed contacts. Because of the nonlocality of the tunneling current it was and partially still is a matter of belief to claim that STM is an “atomic” or “surface” specific experimental tool, whereby even the term surface is a bit misleading, since also buried magnetic structures can be “seen” in STM.

In order to facilitate a direct comparison to experimental data, very recently it was suggested¹² to evaluate directly differences of the tunneling current as an implicit function of the external magnetic field represented theoretically by the corresponding free energy (band-energy contribution to the magnetic anisotropy energy). In using this kind of description it is at least possible to compare the experimentally measured quantity, namely, a dI/dV curve with the applied field as variable, with an equivalent theoretical curve, and to answer questions about the actual meaning of the experimental data.

In this paper “theoretical experiments” are discussed by mimicking vertical and horizontal movements of the tip assuming a rather small Cr/W tip, which was introduced in Ref. 12. Also investigated are changes in the magnetic properties of the system either by considering a small Fe/W system or on the sample side. Particular attention is given to introduce paths on the hypersurface of the anisotropy energy and of the zz -like conductivity tensor elements, a formal scheme that not only allows one to take STM experiments “theoretically” apart, but, in addition, facilitates the evaluation of flipping times along different paths.

II. SYSTEMS INVESTIGATED

For the theoretical experiments discussed in the following a Cu(111) substrate is considered coated with laterally large islands of Fe or Co of different thickness and a Cr/W or Fe/W tip connected to a Cu lead. In particular, the systems listed in Table I are considered. These systems are modeled theoretically by making use of two-dimensional translational symmetry. The sample part consists of the substrate, the magnetic film on top and the adjacent vacuum layer, e.g.,

TABLE I. Systems considered.

a	Cu(111)/Cu _s /Co _m Vac _n /Cr ₃ W ₇ /Cu _l /Cu lead <i>s, l</i> ≥ 12, <i>m</i> ≤ 5, <i>n</i> ≤ 7
b	Cu(111)/Cu ₁₅ /Co ₂ Vac ₃ /Fe ₂ W ₇ /Cu ₁₆ /Cu lead
c	Cu(111)/Cu ₁₅ /Fe ₂ Vac ₃ /Cr ₃ W ₇ /Cu ₁₅ /Cu lead

Cu(111)/Cu₁₅/Co₂Vac₁, where the numbering refers to atomic monolayers (MLs). The tip part comprises the rest of the system, e.g., Vac₂Cr₃W₇/Cu₁₅/Cu lead. In order to vary the width of the vacuum barrier in case (a) *m*=2 and *n*≤7 is chosen; to vary the thickness of the Co layers *n*=3 and *m*≤5. Cases (a) and (b) refer to a Cr/W tip, case (b) to an Fe/W tip. Both, the tip and the sample are semi-infinite systems, the Cu_s on the sample side and the Cu_l layers on the tip side are additional Cu layers to guarantee a smooth joining up with the bulklike substrate and the lead. It should be noted that in the present approach not two surfaces are considered but a single infinite system with two semi-infinite parts.

The magnetic properties in the sample part are characterized by one uniform orientation of the magnetization confined to the *xz* plane as defined by an angle Θ_1 , those in the tip part by another uniform direction corresponding to Θ_2 , where Θ_1 and Θ_2 are rotation angles around the in-plane *y* axis. The *z* axis is parallel to the surface normal, i.e., is parallel to (111). It will be shown that in certain cases also the orientation of the magnetization in other layers such as in the vacuum barrier has to be varied separately.

III. THEORETICAL APPROACH

A. Free-energy hypersurface

The (experimentally applied) external magnetic field, assumed as used in most experiments to be parallel or antiparallel to the surface normal, is proportional to the following band-energy contribution (grand canonical potential, free energy at zero temperature) to the magnetic anisotropy energy,

$$E_b(\Theta_1, \Theta_2; d_{\text{Co}}, d_{\text{vac}}) = E(\Theta_1, \Theta_2; d_{\text{Co}}, d_{\text{vac}}) - E(0, 0; d_{\text{Co}}, d_{\text{vac}}), \quad (1)$$

where Θ_1 and Θ_2 , in principle, can vary between 0° and 180°; d_{Co} and d_{vac} refer to the thickness of a Co island and the width of the vacuum barrier, respectively, and $E(\Theta_1, \Theta_2; d_{\text{Co}}, d_{\text{vac}})$ is given by^{13,14}

$$E(\Theta_1, \Theta_2; d_{\text{Co}}, d_{\text{vac}}) = \sum_{i=1}^L E^i(\Theta_1, \Theta_2; d_{\text{Co}}, d_{\text{vac}}), \quad (2)$$

$$E^i(\Theta_1, \Theta_2; d_{\text{Co}}, d_{\text{vac}}) = \int_{E_0}^{E_F} n^i(\Theta_1, \Theta_2; d_{\text{Co}}, d_{\text{vac}}; z) \times (z - E_F) dz. \quad (3)$$

In Eq. (2) *L* refers to the total number of atomic layers considered; in Eq. (3) E_0 and E_F denote the valence-band bottom and the Fermi energy, *z* a complex energy, and

$n^i(\Theta_1, \Theta_2; d_{\text{Co}}, d_{\text{vac}}; z)$ is the density of states in the *i*th atomic plane for a particular choice of Θ_1 , Θ_2 , d_{Co} , and d_{vac} . The $E^i(\Theta_1, \Theta_2; d_{\text{Co}}, d_{\text{vac}})$ are so-called layer-resolved band energies. The band energy in Eq. (1) is defined with respect to a reference configuration in which the orientation of the magnetization is uniformly perpendicular to the planes of atoms through the whole system (sample and tip).

It should be noted that at given values of d_{Co} and d_{vac} the band energy $E_b(\Theta_1, \Theta_2; d_{\text{Co}}, d_{\text{vac}})$ forms a surface in a function space spanned by Θ_1 and Θ_2 . Keeping one of the angles constant and varying the other one, implies taking a particular path on this surface. For example, varying for $\Theta_2=0$ the angle Θ_1 between 0° and 90° means to follow the path, denoted in the following as $[\Theta_1, 0]$, that leads to an eventual reorientation transition of the magnetic parts of the sample from perpendicular to in plane, while the magnetization in the tip remains perpendicularly oriented to the surface. Similarly, when varying Θ_2 at $\Theta_1=90^\circ$ a path $[90, \Theta_2]$ is followed that corresponds entirely to a change in the orientation of the magnetization in the tip while the sample is in an in-plane configuration. According to these paths, for matters of simplicity the below contracted notation shall be used

$$E_b(\Theta_1, \Theta_2; d_{\text{Co}}, d_{\text{vac}}) = \begin{cases} E^{(0)}(d_{\text{Co}}, d_{\text{vac}}); & [\Theta_1, \Theta_2] \\ E^{(1)}(d_{\text{Co}}, d_{\text{vac}}); & [\Theta_1, 0] \\ E^{(2)}(d_{\text{Co}}, d_{\text{vac}}); & [90, \Theta_2], \end{cases} \quad (4)$$

$$k=0: 0 \leq \Theta_1, \Theta_2 \leq 180$$

$$k=1: 0 \leq \Theta_1 \leq 90$$

$$k=2: 0 \leq \Theta_2 \leq 180, \quad (5)$$

where $[\Theta_1, \Theta_2]$ denotes a general path on the band-energy surface.

One easily can imagine that by considering more than two rotation angles as variables a surface of higher order (hypersurface) has to be investigated. It is important to note that subsequent rotations of the orientation of the magnetization in particular layer(s) are independent from each other,¹⁵ i.e., it does not matter whether first a rotation of the orientation of the magnetization corresponding to a rotation angle Θ_1 is performed and then one with respect to Θ_2 , or oppositely.

B. Electric currents

Since the experimentally applied current is parallel or antiparallel to the surface normal the relevant electric conductivity tensor corresponding to Θ_1 , Θ_2 , d_{Co} , and d_{vac} , is given¹⁴ by its *zz* element,

$$\sigma_{zz}(\Theta_1, \Theta_2; d_{\text{Co}}, d_{\text{vac}}) = L^{-1} \sum_{i,j=1}^L \sigma_{zz}^{ij}(\Theta_1, \Theta_2; d_{\text{Co}}, d_{\text{vac}}), \quad (6)$$

where the $\sigma_{zz}^{ij}(\Theta_1, \Theta_2; d_{\text{Co}}, d_{\text{vac}})$ are the layer-wise matrix elements of the *zz*-like conductivity tensor and *L* now also takes up the meaning of the distance (in ML) separating the electric contacts. Assuming that the *z* component of the electric field, E_z , is uniform in all atomic layers,¹⁶ the local and

the total currents¹⁷ can be considered to be directly proportional to the respective conductivities,

$$j_z(\Theta_1, \Theta_2; d_{Co}, d_{vac}) = \sum_{i=1}^L j_z^i(\Theta_1, \Theta_2; d_{Co}, d_{vac}), \quad (7)$$

$$j_z^i(\Theta_1, \Theta_2; d_{Co}, d_{vac}) = \frac{E_z}{L} \sum_{j=1}^L \sigma_{zz}^{ij}(\Theta_1, \Theta_2; d_{Co}, d_{vac}). \quad (8)$$

Per definition the layer-resolved (local) currents, $j_z^i(\Theta_1, \Theta_2; d_{Co}, d_{vac})$, need not all to be positive, only the total current has to fulfill this property. Clearly enough for given values of d_{Co} and d_{vac} the values of $\sigma_{zz}(\Theta_1, \Theta_2; d_{Co}, d_{vac})$ and consequently also of $j_z(\Theta_1, \Theta_2; d_{Co}, d_{vac})$ generate again a surface in the function space spanned by Θ_1 and Θ_2 . In order to compare with experimental data it is useful to define in a similar manner as for the band-energy conductivities $\sigma_{zz}(\Theta_1, \Theta_2; d_{Co}, d_{vac})$ and difference conductivities $\Delta\sigma_{zz}(\Theta_1, \Theta_2; d_{Co}, d_{vac})$ along particular paths,

$$\sigma_{zz}(\Theta_1, \Theta_2; d_{Co}, d_{vac}) = \begin{cases} \sigma^{(0)}(d_{Co}, d_{vac}); & [\Theta_1, \Theta_2] \\ \sigma^{(1)}(d_{Co}, d_{vac}); & [\Theta_1, 0] \\ \sigma^{(2)}(d_{Co}, d_{vac}); & [90, \Theta_2], \end{cases}$$

$$\Delta\sigma_{zz}(\Theta_1, \Theta_2; d_{Co}, d_{vac}) = \begin{cases} \Delta\sigma^{(0)}(d_{Co}, d_{vac}); & [\Theta_1, \Theta_2] \\ \Delta\sigma^{(1)}(d_{Co}, d_{vac}); & [\Theta_1, 0] \\ \Delta\sigma^{(2)}(d_{Co}, d_{vac}); & [90, \Theta_2]. \end{cases} \quad (9)$$

where $\Delta\sigma^{(0)}(d_{Co}, d_{vac})$ describes the changes in the conductivity $\sigma_{zz}(\Theta_1, \Theta_2; d_{Co}, d_{vac})$ along a general path with respect to the reference configuration $\Theta_1, \Theta_2=0$, $\Delta\sigma^{(1)}(d_{Co}, d_{vac})$ such changes along path $[\Theta_1, 0]$, and $\Delta\sigma^{(2)}(d_{Co}, d_{vac})$ along $[90, \Theta_2]$, however, with respect to the conductivity at $\Theta_1=90, \Theta_2=0$. The first difference conductivity, $\Delta\sigma^{(0)}(d_{Co}, d_{vac})$, has to be regarded as a kind of global contrast, the other ones split up this contrast into two parts, one according to changes to be experienced in turning the orientation in the magnetic overlayer, the second, following one reflects the changes in contrast entirely caused by the orientation of the magnetization in the tip part of the system. The corresponding local difference conductivities (currents) are denoted in the following by $\Delta\sigma^{(k),i}(d_{Co}, d_{vac})$, where k refers to the path and i to the atomic layer.

Finally, since for any given values of Θ_1 and Θ_2 one can associate to $\sigma_{zz}(\Theta_1, \Theta_2; d_{Co}, d_{vac})$ the corresponding value of the band energy $E_b(\Theta_1, \Theta_2; d_{Co}, d_{vac})$, differences in the local and the total currents along a particular path can be viewed as implicit functions along the same path on the band-energy surface,

$$\Delta\sigma_{zz}^{(k)}(E_b; d_{Co}, d_{vac}) = \sum_{i=1}^L \Delta\sigma^{(k),i}(E_b; d_{Co}, d_{vac}), \quad (10)$$

where as before k specifies the path.

C. Time scales

One additional remark has to be made before going ahead discussing various applications. Viewed in terms of the Landau-Lifshitz-Gilbert equation the curvature of $E_b(\Theta_1, \Theta_2; d_{Co}, d_{vac})$ along a particular path can be used to evaluate the time needed for the system to switch from one magnetic configuration to another one.¹⁸ Going along path $[\Theta_1, 0]$ or path $[90, \Theta_2]$ leads as will be shown later on to quite different characteristic times (switching times) to be associated with these paths. As presently spin-polarized STM experiments are performed time integrated this particular feature will not be reflected directly in the experimental data, it can, however, provide additional understanding in interpreting experiments. In perhaps future time-resolved spin-polarized STM experiments such characteristic times will definitely play an important role.

IV. COMPUTATIONAL APPROACH

All *ab initio* electronic-structure calculations were performed at the experimental lattice constant of Cu (interlayer distance 2.087 Å) for a uniform direction of the magnetization pointing along the surface normal in terms of the spin-polarized (fully) relativistic screened Korringa-Kohn-Rostoker method.¹³ The band energies in Eq. (1) are evaluated (at zero temperature) in terms of the magnetic force theorem¹⁴ by integrating in the upper half of the complex energy plane along a contour starting at E_0 and ending at the Fermi energy, see Eq. (3). The electric transport properties were evaluated by means of the fully relativistic Kubo-Greenwood equation,¹⁴ the Landau-Lifshitz-Gilbert equation was solved using the approach and the approximations discussed in Ref. 18. In all calculations a maximum angular quantum number of two,¹³ the density-functional parametrization of Ref. 19, and the atomic sphere approximation were used.

V. Co ISLANDS ON Cu(111)

A. Vertical movements of the tip

Suppose there is a Co island, 2 ML high on Cu(111), large enough to be described by two-dimensional translational symmetry. One of the very first theoretical questions that arises is what happens if the width of the vacuum barrier is changed, i.e., when performing a “vertical” movement of the tip ($\text{Cr}_3\text{W}_7\text{Cu}$ lead). From Fig. 1 it is apparent that the band energy $E_b(90, 0; d_{Co}, d_{vac})$, namely, the energy difference between an in plane and a perpendicular arrangement of the magnetization in the Co layers, quickly becomes a constant as the width of the barrier increases, and that the corresponding zz -like conductivities fall off exponentially (indicated by a dashed line showing an exponential fit through the calculated values). The values of the layer-resolved difference conductivities $\Delta\sigma^{(1),i}(d_{Co}, d_{vac})$ (left entry in the lower part of Fig. 1) for particular layers i prove that independent of the width of the vacuum barrier the top Co layer contributes most to the total difference conductivity $\Delta\sigma^{(1)}(d_{Co}, d_{vac})$. It is interesting to note that both the first Cu layer as well as the first vacuum layer do add considerably to the total difference

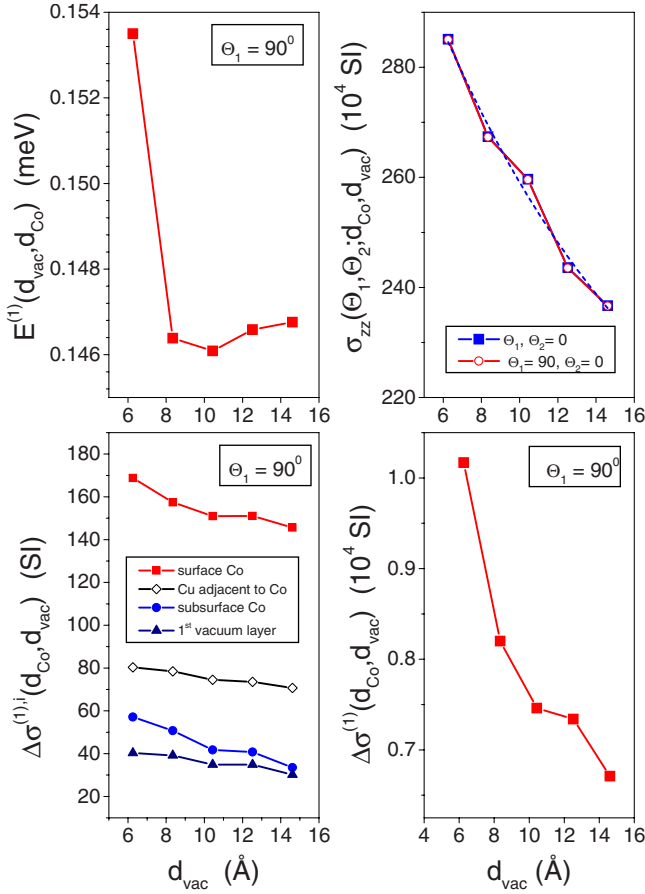


FIG. 1. (Color online) Cu(111)/Co₂Vac_nCr₃W₇/Cu lead. Top: band energy (left) and configuration-dependent zz elements of the conductivity tensor (right). Bottom: peak values in the local difference conductivity, right: (total) difference conductivity, for definitions, see text. All data are shown as functions of the width of the vacuum barrier. The dashed line in the top right entry refers to a fit with respect to an exponential decay. Θ_1 and Θ_2 are marked explicitly.

conductivity (right entry in the lower part of Fig. 1). From the latter quantity follows immediately that with increasing width of the vacuum barrier it becomes increasingly difficult to trace experimentally a reorientation transition. Clearly enough, most of the results shown in Fig. 1 are pretty much what was to be expected.

It should be noted that in Fig. 1 only differences between an in plane and a perpendicular arrangement of the magnetization in the sample are displayed since the actual dependence on Θ_1 at a given value for d_{vac} along the path $[\Theta_1, 0]$ was already shown in Ref. 12.

B. Changing the thickness of the Co islands

Suppose there are laterally large Co islands of different thicknesses, the width of the vacuum barrier is kept constant at about 6 Å (3 ML), and a Cr₃W₇ tip is used. Again the emphasis shall be put only on the difference between an in plane and a perpendicular orientation of the magnetization in the Co islands, i.e., on the difference between the end points along the path $[\Theta_1, 0]$. From the top part of Fig. 2 follows

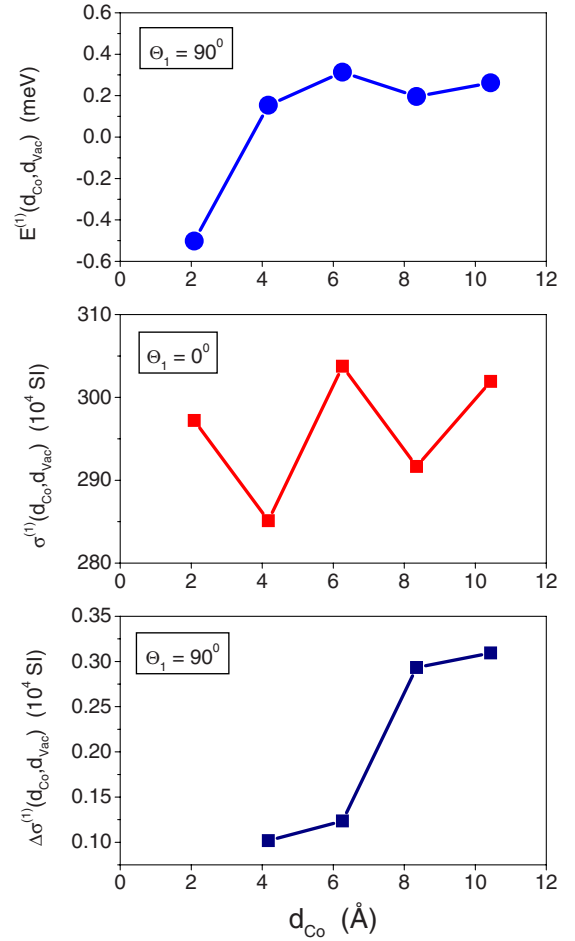


FIG. 2. (Color online) Cu(111)/Co_nVac₃Cr₃W₇/Cu lead. Band energy (top), conductivity (middle), and difference conductivity (bottom) shown as functions of the thickness of the Co overlayer. For definitions, see text. Θ_1 is marked explicitly.

that with increasing thickness of the Co film the band energy as well as the zz -like conductivities start to oscillate with respect to the Co thickness. Such oscillations with a period of two are already quite well known from the literature, see, e.g., Ref. 20.

The interesting new feature, however, is that for a Co thickness of larger than 5 Å (3 ML's) the penultimate Co layer becomes more important than the top Co layer, which in turn explains the changes in the total difference conductivity (Fig. 2, bottom). This peculiar feature is also already known from the literature²¹ and is best understood in viewing the layer-resolved band energies as defined in Eq. (3) (top part of Fig. 3) and the layer-resolved difference conductivities (Fig. 3, bottom) in the vicinity of the Co/Vac interface. Obviously once the main peak in the layer-resolved band energies no longer is situated in the top Co layer, but moved in the interior of the Co islands, then also the decay of the local difference conductivities into the interior of the substrate is much slower. Figure 2 does indeed have consequences for experimental studies: for Co islands higher than 3 ML structural views will reflect only partially the top Co layer, i.e., a clearly defined determination of a “surface structure” will become meaningless.

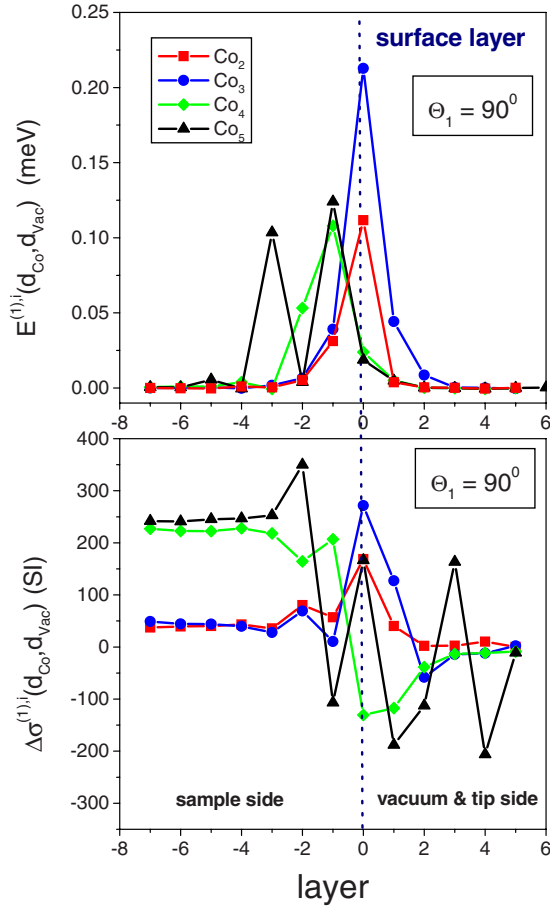


FIG. 3. (Color online) Cu(111)/Co_nVac₂Cr₃W₇/Cu lead. Layer-resolved band energies (top) and difference conductivities (bottom) in the vicinity of the top Co layer. Θ_1 is marked explicitly. The dashed vertical line refers to the top Co layer.

C. Viewing Co islands of different thickness

The most complicated case arises when moving the tip horizontally over Co islands of different thicknesses since the Co thickness as well as the width of the vacuum barrier changes. Investigated in the following are cases in which the thickness of the Co/Vac interface in ML, $/\text{Co}_n\text{Vac}_m/$, remains constant ($n+m=5$). Again a Cr₃W₇ tip is assumed, and only respective differences between an in plane and a perpendicular orientation of the magnetization in the Co islands are considered.

Although the band energy in Fig. 4 seems to be as one would expect at a first glance, namely, a reorientation transition occurs between one and two ML of Co,²² there is a strong increase in the conductivity as the width of the vacuum barrier approaches 4 Å. Consequently also the difference conductivity varies strongly. The reason for this kind of behavior can easily be read off from the distribution of charges in the atomic layers forming the vacuum barrier, see the bottom left entry of Fig. 4. Obviously at 4 Å the sample and the tip are already electrically connected, i.e., the whole system shows (ordinary) metallic conductivity.

Being mainly interested in recording the switching properties of Co islands, from Figs. 1 and 4 follows that these

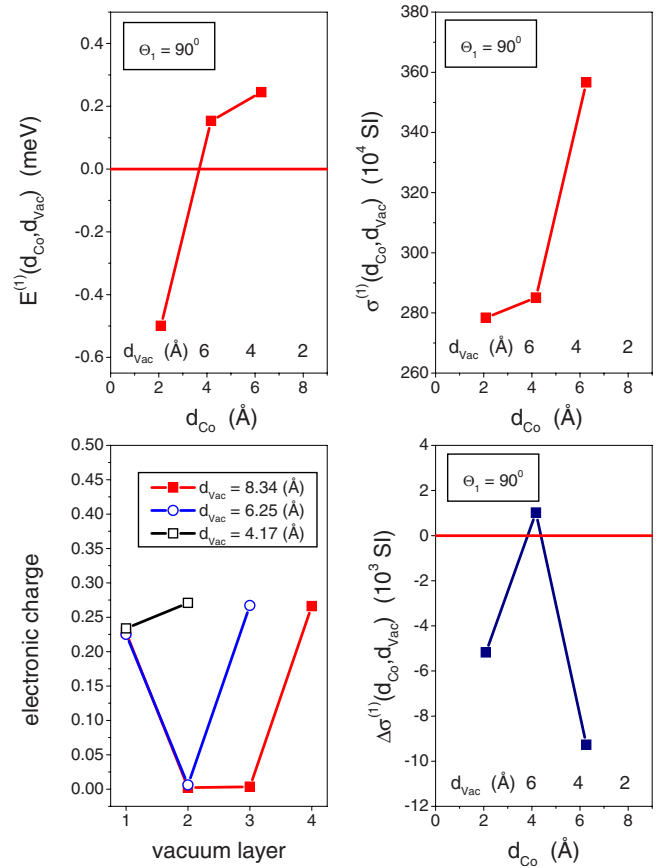


FIG. 4. (Color online) Cu(111)/Co_nVac_mCr₃W₇/Cu lead. Band energy (top, left), conductivity (top, right), and difference conductivity (bottom, right). For definitions, see text. Θ_1 is marked explicitly. Bottom left: electronic charge in the vacuum layers for different widths (indicated) of the vacuum barrier.

islands should be 2–3 ML high and the optimal width of the vacuum barrier is between about 6 and 8 Å. For a vacuum barrier of well above 8 Å the resolution might become a problem, below 6 Å the electric contact of the sample with the tip most likely will turn out to be a severe problem.

VI. DECOUPLING THE ORIENTATION OF THE MAGNETIZATION OF THE SURFACE STATE

Suppose the external magnetic field is increased beyond the combined value of the band energy of the sample and the tip, then the question arises into what kind of magnetic rearrangement the system is forced by such an increase. In order to answer this particular question one has to investigate not only variations in the orientation of the magnetization in the sample and in the tip but also, for example, in the vacuum layers. Considering again a laterally large Co island, 2 ML high ($d_{\text{Co}}=4.17$ Å), a vacuum barrier with a width of about 3 ML ($d_{\text{vac}}=6.25$ Å), and a Cr₃W₇ tip, then by allowing for more rotational degrees of freedom the band energy has to be redefined, for example, as

$$E_b(\Theta_1, \Theta_2; \varphi_1, \varphi_2, \varphi_3) = E(\Theta_1, \Theta_2; \varphi_1, \varphi_2, \varphi_3) - E(0, 0; 0, 0, 0),$$

where φ_1 , φ_2 , and φ_3 are again rotations angles around the in plane y axis. The angle φ_1 refers to the vacuum layer next to

TABLE II. Value of the band energy (millielectron volt) necessary to flip the orientation in a 2 ML high Co island on Cu(111) from perpendicular to in plane using either Cr/W tips or an Fe/W tip. The value for a free surface of 2 ML Co on Cu(111) is 0.1468 meV (Ref. 22).

Θ_1	Θ_2	Cr ₃ W ₇ tip	Cr ₁₅ W ₂₂ tip	Fe ₂ W ₇ tip
90	0	0.1536	0.1515	0.1966
0	90	0.0436	-0.0002	0.1746
90	90	0.1761	0.1432	0.2622

Co, φ_3 to that next to Cr, and φ_2 to the vacuum layer in between. In a similar manner, a corresponding difference conductivity $\Delta\sigma_{zz}(\Theta_1, \Theta_2; \varphi_1, \varphi_2, \varphi_3; d_{Co}, d_{vac})$ can be defined. However, since for a Cr₃W₇ tip the band-energy contribution from the tip is rather small, see also Table II, it seems save to assume that only the vacuum layer next to Co is of importance. In Fig. 5 the band energy and the difference conductivity are displayed when Θ_1 , Θ_2 , and φ_1 vary. Note that in this figure the different regimes separated by vertical lines actually refer to different paths $[\Theta_1, \Theta_2, \varphi_1]$ on hypersurfaces in the function space spanned by these three angles.

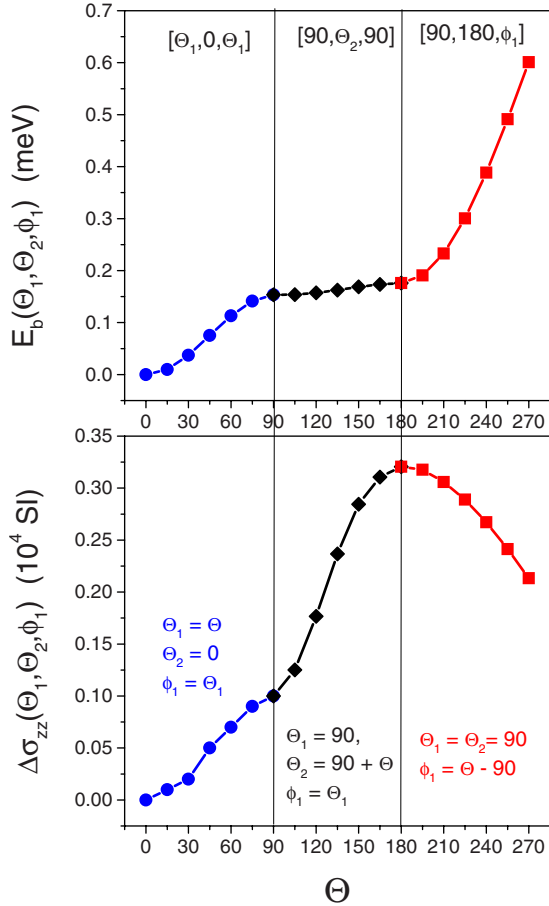


FIG. 5. (Color online) Cu(111)/Co₂Vac₃Cr₃W₇/Cu lead. Band energy (top) and difference conductivity (bottom) as a function of Θ_1 , Θ_2 , and φ_1 . The paths on the band-energy hypersurface are marked explicitly. Note that in order to have a two-dimensional projection it is necessary to mark the actual angles explicitly.

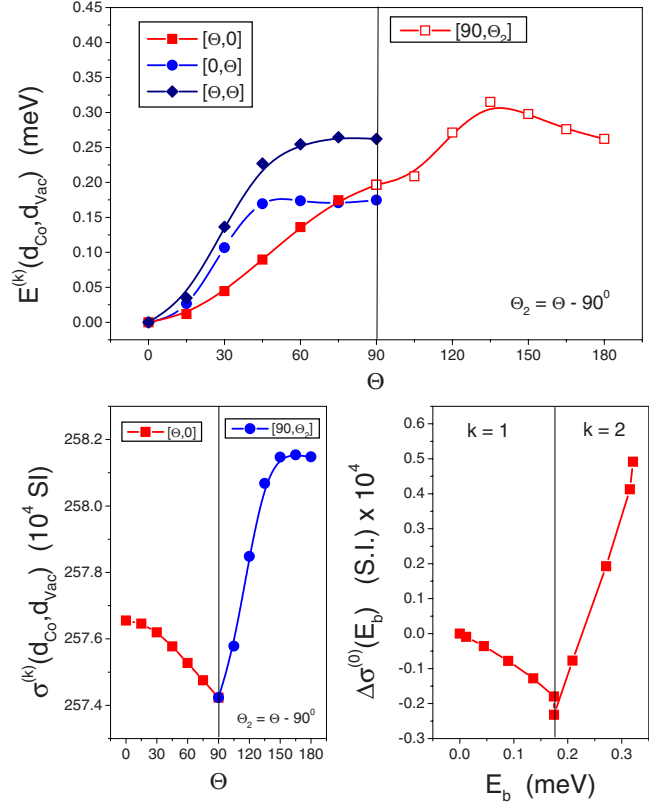


FIG. 6. (Color online) Cu(111)/Co₂Vac₃Fe₂W₇/Cu lead. Band energy (top) and zz -like conductivity (bottom, left) for various paths (indicated). Bottom, right: difference conductivity as an (implicit) function of the band energy.

As can be seen, by starting from a uniform perpendicular orientation of the magnetization ($\Theta_1=0$, $\Theta_2=0$, $\varphi_1=0$) along the path $[\Theta_1, 0, \Theta_1]$, first the Co layers switch the orientation of the magnetization, then along $[90, \Theta_2, 90]$ the orientation of the magnetization in the tip is rearranged. The latter effect is indeed very small and does depend on the type of tip, as is shown later on in Table II. Finally, at even higher fields the orientation in the first vacuum layer (surface state) changes; along the path $[90, 90, \varphi_1]$ it becomes decoupled from the orientation of the magnetization in the Co layers until it is finally perpendicular to that in the Co layers. This end point corresponds to a band energy that is four times as large as the energy that is needed to switch the orientation of the magnetization in the Co layers from perpendicular to in plane. The figure for the difference conductivity shows that this quantity is strongly increased when orienting the direction of the magnetization in the tip perpendicularly to that in the Co layers; decoupling the “surface state” then reduces the difference conductivity at high enough external fields.

Changing the magnetic properties of the tip

Suppose now that the Cr₃W₇ tip assumed up to now is replaced by an Fe₂W₇ tip and investigated is once again a large Co island, 2 ML high using a tip/sample separation of about 6 Å (3 ML). From the top entry in Fig. 6 one can see that up to about $\Theta_1 \approx 75^\circ$ the band energy for changing the

orientation in the Co layers is the smallest one and that a uniform rotation in the sample and the tip ($\Theta_1, \Theta_2 = \Theta$) leads to a quite a bit higher band energy. At about $75^\circ \leq \Theta \leq 90^\circ$, however, two paths, namely, $[\Theta_1, 0]$ and $[0, \Theta_2]$, intersect, i.e., respective band energies become equally probable. Varying additionally for an in-plane orientation of the magnetization in the Co layer the orientation in the tip, i.e., following the path $[90^\circ, \Theta_2]$, leads to a further increase in band energy and eventually to a maximum at about $\Theta_2 = 135^\circ$. It is obvious that the reorientation transition in the Co layers can still be determined without ambiguities, see in the bottom entries of Fig. 6 the sharp minimum with respect either to Θ or E_b .

Quite obviously the band energy at which an in-plane orientation of the Co islands is reached does indeed depend on the type of tip used, see Table II. Although, in particular, for $\Theta_1 = 90^\circ, \Theta_2 = 0$, in this table the differences might appear to be rather small, they indicate that any kind of experimental “determination” of the anisotropy energy does indeed depend (slightly) on the tip used. Clearly enough, if needed, the origin of the small differences in band energy with respect to different tips can easily be explained using again the concept of layer-resolved band energies.

VII. Fe ISLANDS ON Cu(111) USING A Cr_3W_7 TIP

As a last example a case is studied in which the Co islands are replaced by 2 ML high Fe islands and the same Cr_3W_7 tip (and sample/tip separation) is considered as before. In Fig. 7 again the band energy $E^{(k)}(d_{\text{Co}}, d_{\text{Vac}})$ and the conductivity $\sigma^{(k)}(d_{\text{Co}}, d_{\text{Vac}})$ are displayed along $[\Theta_1, 0]$ and $[90, \Theta_2]$ as well as $\Delta\sigma_{zz}^{(0)}(E_b)$. Although the band energy seems to be of the same shape as the one in the first two regimes displayed in Fig. 5, once the system is in configuration $(90, \Theta_2)$ and Θ_2 is varied the total and the difference conductivity drop considerably, thus causing a sudden break in $\Delta\sigma_{zz}^{(0)}(E_b)$, see the bottom entry in Fig. 7.

VIII. COMPARISON TO EXPERIMENT, TIME SCALES

Disregarding the in-plane anisotropy, which for magnetic overlayers usually is by at least one order of magnitude smaller than the out-of-plane anisotropy,¹⁸ the surface of the band energy can be thought of as a three-dimensional body generated by rotating the paths $[\Theta_1, 0]$ and $[90, \Theta_2]$ around the surface normal. Inspecting, e.g., the first two regimes in Fig. 5, it is easy to see that this rotational body almost looks like a plate with a rather flat rim. In order to estimate how long it takes to reach the rim and then to cross the rim, i.e., to move along path $[\Theta_1, 0]$ from $\Theta_1 = 0$ to $\Theta_1 = 90^\circ$, and then along $[90, \Theta_2]$ by varying Θ_2 between 0 and 90, one can use the approach to solve the Landau-Lifshitz-Gilbert equation introduced in Ref. 18, since along each of these paths only one particular rotation of the magnetization is varied. Considering for 2 ML high extended islands of Co on Cu(111) only either the two Co layers or the Cr layers in the tip and by replacing in these two slabs the magnetic moments by a single magnetic moment averaged over the number of atomic layers in each of these slabs, one arrives at the times listed in Table III.

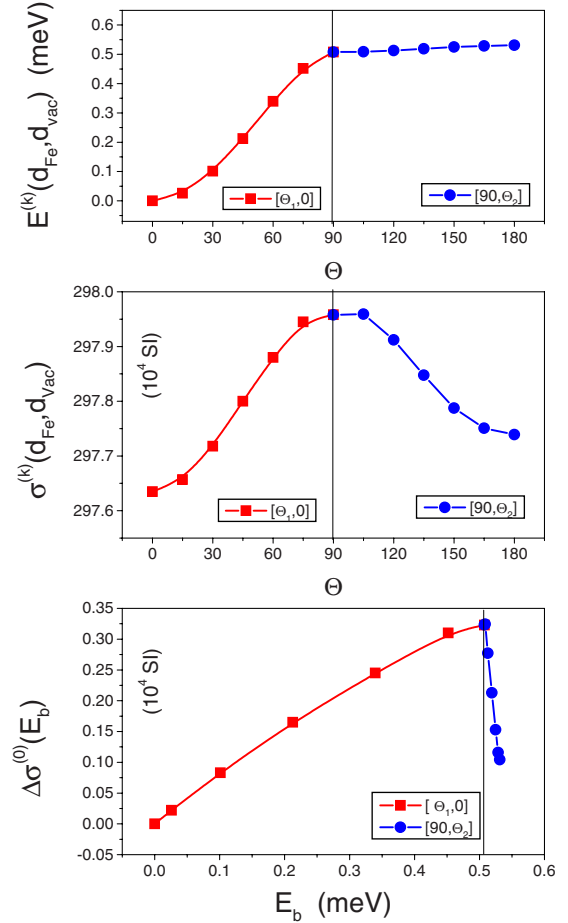


FIG. 7. (Color online) Cu(111)/ $\text{Fe}_2\text{Vac}_3\text{Cr}_3\text{W}_7/\text{Cu}$ lead. Band energy (top) and conductivity (middle), and difference conductivity as a function of the band energy. The paths on the band-energy hypersurface are marked explicitly. Note that for plotting purposes in this figure $\Delta\sigma_{zz}(\Theta_1, \Theta_2)$ is multiplied by -1 .

As can be seen from this table in the case of Co islands by using a Cr_nW_m tip the “switching time” along $[90, \Theta_2]$, namely, for the Cr layers, is typically at least one order of magnitude smaller than those along $[\Theta_1, 0]$, for a Fe_2W_7 tip, however, the switching of the Fe layers in the tip (τ_2) is by two orders of magnitude slower than the switching time for the Co islands (τ_1). Only in the case of 2 ML high Fe islands these two switching times are of the same magnitude.

TABLE III. Switching times for various samples and tips along particular paths, $0 \leq \Theta_1, \Theta_2 \leq 90$.

Sample	Tip	Path	Type	(ps)
Co ₂	Cr ₃ W ₇	$[\Theta_1, 0]$	τ_1	0.58×10^2
		$[90, \Theta_2]$	τ_2	0.56×10^0
Co ₂	Cr ₁₇ W ₂₂	$[\Theta_1, 0]$	τ_1	0.58×10^2
		$[90, \Theta_2]$	τ_2	0.33×10^1
Co ₂	Fe ₂ W ₇	$[\Theta_1, 0]$	τ_1	0.40×10^2
		$[90, \Theta_2]$	τ_2	0.19×10^4
Fe ₂	Cr ₃ W ₇	$[\Theta_1, 0]$	τ_1	0.90×10^1
		$[90, \Theta_2]$	τ_2	0.27×10^1

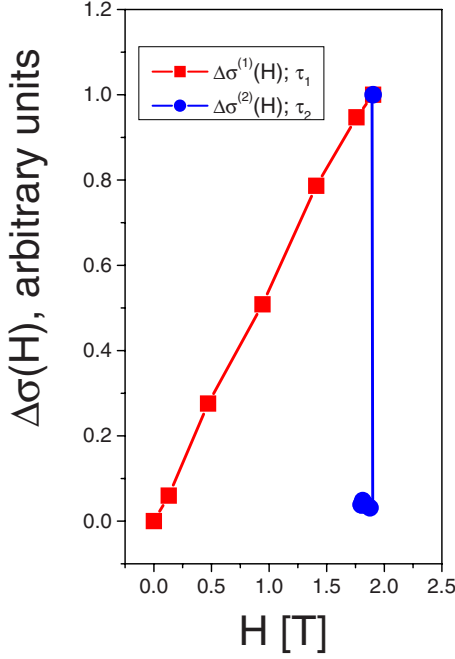


FIG. 8. (Color online) Cu(111)/Co₂Vac₃Cr₁₅W₂₂/Cu lead. Difference conductivities as a function of the applied field (T). Squares refer to path $[\Theta_1, 0]$, diamonds and spheres to path $[90, \Theta_2]$. Note the abrupt change in $\Delta\sigma^{(2)}(H)$ at about 1.7 T.

Clearly enough, although based on *ab initio* determined band energies, the times listed in Table III can only be regarded at best as estimates. However, as summarized below they do indicate that once the reorientation transition in the magnetic overlayer is reached the contrast to be seen beyond this point most likely is governed by τ_2 ,

$$\Delta\sigma_{zz}(\Theta_1, \Theta_2; d_M, d_{vac}) = \begin{cases} \Delta\sigma^{(0)}(d_M, d_{vac}), 0 \leq t \leq (\tau_1 + \tau_2), & \tau_1 \sim \tau_2 \\ \Delta\sigma^{(1)}(d_M, d_{vac}), 0 \leq t \leq \tau_1, & \tau_1 \gg \tau_2, \\ \Delta\sigma^{(2)}(d_M, d_{vac}), \tau_1 \leq t \leq (\tau_1 + \tau_2), & \tau_1 \gg \tau_2, \end{cases}$$

M being either Co or Fe. If $\tau_2 \gg \tau_1$ a switching of the orientation of the magnetization in the tip seems unlikely to occur. Comparing the bottom entry of Fig. 7 with Fig. 8, one can see that if $\tau_1 \sim \tau_2$ the global difference conductivity $\Delta\sigma^{(0)}(d_M, d_{vac})$ yields an abrupt change when passing beyond the point at which the reorientation transition is reached, while for $\tau_1 \gg \tau_2$ such an abrupt change is only the case if viewed in terms of $\Delta\sigma^{(2)}(d_M, d_{vac})$ and as listed in Table II the variation in the band energy along $[90, \Theta_2]$ is very small indeed, see the entry headed by Cr₁₅W₂₂ tip. As an illustration in Fig. 8 the paths corresponding to τ_1 and τ_2 are shown when using this particular tip. This figure can now directly be compared to the data shown in Ref. 1 for which a Cr/W tip with a (roughly) comparable Cr thickness was used.²³

IX. SUMMARY AND CONCLUSION

Perhaps the best way to summarize one of the main topics discussed in here is to show yet another figure. In Fig. 9 the

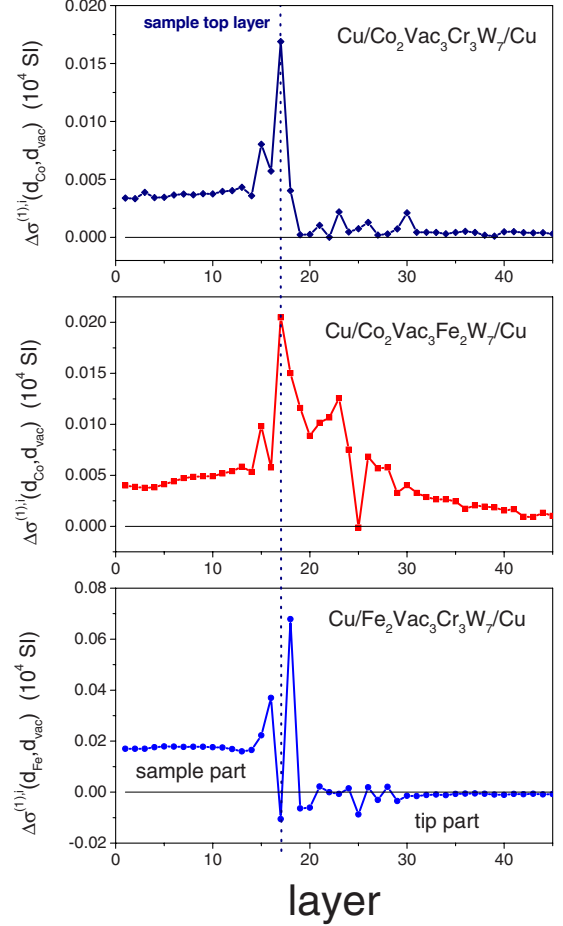


FIG. 9. (Color online) Layer-resolved zz -like difference conductivities for a two ML high overlayer of Co on Cu(111) using a Cr₃W₇ (top) and an Fe₂W₇ (middle) tip. Bottom: two ML high overlayer of Fe on Cu(111) using a Cr₃W₇ tip. The position of the surface layer is marked by a vertical dotted line.

layer-resolved difference conductivities in three different systems are compared with. The top two entries show the effect of changing the tip, the bottom one of changing the magnetic overlayer. It can be easily seen that for 2 ML of Co on Cu(111) by using a Cr₃W₇ tip and a vacuum barrier of about 6 Å the main contribution to the difference in the conductivity between an in plane and a perpendicular arrangement of the magnetization in the Co layer arises from the top Co layer, while with an Fe₂W₇ tip the Co layers as well as the vacuum barrier and the tip contribute, see also Fig. 6. In the case of 2 ML of Fe on Cu(111), however, not the Fe layers are seen but the first vacuum layer (surface state). This obviously is also the reason for the above mentioned break in $\Delta\sigma^{(0)}(E_b)$ with respect to E_b shown in Fig. 7 and why $\tau_1 \sim \tau_2$.

In order to bridge the present method with approaches based on Tersoff and Hamann⁶ it has to be recalled that since two-dimensional translational symmetry was assumed also the local conductivities $\sigma^{(k),i}(d_{Co}, d_{vac})$ are two-dimensional translationally invariant, explaining thus in turn the regular pattern seen when moving the tip horizontally over an extended island. Furthermore, they are also invariant with respect to the applying two-dimensional rotational symmetry

group. In principle, they even can be evaluated spatially resolved as $\sigma^{(k),i}(\mathbf{r}_i; d_{\text{Co}}, d_{\text{Vac}})$ simply by not integrating the current matrices¹⁴ over the volume of the Wigner-Seitz cell characteristic for the i th atomic layer. In short, the $\sigma^{(k),i}(d_{\text{Co}}, d_{\text{Vac}})$ can be made to look like the quantities usually evaluated, however, they still represent the local contributions to a well-defined tunneling current.

It has to be mentioned that experimentally very often a change in the bias voltage is used in order to record a differential tunneling current. A high enough bias voltage can even cause a current-induced switching of the orientation(s) of the magnetization in the system. This mode of operation makes an interpretation of corresponding data by no means easier since then also additional torques caused by the interaction of the system with an external electromagnetic field have to be taken into account, see, for example, Ref. 24.

It is evident that in all cases in which the contribution from the tip to the switching energy is small or even negligible structural relaxations (neglected in the present calculations) in the surface near region of the sample are likely to be important. However, even this—in the first place—obvious statement has to be put in proper context, since, as Fig. 3 showed, not always the surface layer is the most important one. The tunneling current is a nonlocal quantity that only in a theoretical approach can be viewed in terms of a sum over local contributions, effects of structural relaxations will therefore depend very much on the type of system investigated (thickness of islands, etc.). Note that of course, in principle, the local and the total currents can be evaluated taking into account surface relaxations and/or by using a full potential scattering approach, for formal details, see Ref. 13

Furthermore, the geometrical shape and composition of the tip clearly are of quite some relevance, in particular, in all experimental studies in which the contribution from the tip to the switching energy may be of relevance. Once one deals

with very small islands or even small clusters of magnetic atoms on suitable substrates also their size and shape become of crucial importance since then the anisotropy energy of rim and edge atoms is “visibly” different from interior ones.^{25,26} For a theoretical description of very small islands definitely a real-space realization of the present approach is needed for both, the anisotropy energy²⁵ and the Kubo-Greenwood equation.²⁷ Then even tunneling currents and the switching properties of individual atoms can be investigated theoretically.

In this context it has to be mentioned that not always an external magnetic field is needed to record STM images of magnetic nanostructures. In principle, it is sufficient that the orientation of the magnetization changes locally such as, for example, in antiferromagnetically ordered overlayers, in “spin spirals,” or domain walls. An impressive example of spin spirals is shown, for example, in Ref. 28. For spin spirals or domain walls, according to Eq. (8), it is sufficient to display the layer-wise contributions to the total domain-wall resistivity discussed already for magnetic alloys with reference to race track memories.²⁹

Finally, it is worthwhile to mention that for the present theoretical approach it does not matter whether the external magnetic field points along the surface normal or not: also so-called in-plane anisotropies in energy and in the corresponding conductivities can be accounted for simply by adding further dimensions (caused by additional rotational freedom) to the band energy and conductivity hypersurfaces.

ACKNOWLEDGMENTS

I am grateful to the Max-Planck-Institut für Mikrostrukturphysik in Halle (Germany), in particular, to J. Kirschner and D. Sander for the discussions we had on this topic, but also for all the computational facilities and help provided.

¹G. Rodary, S. Wedekind, D. Sander, and J. Kirschner, *Jpn. J. Appl. Phys.* **47**, 9013 (2008).

²T. Balashov, T. Schuh, A. F. Takács, A. Ernst, S. Ostanin, J. Henk, I. Mertig, P. Bruno, T. Miyamachi, S. Suga, and W. Wulfhekel, *Phys. Rev. Lett.* **102**, 257203 (2009).

³F. Meier, L. Zhou, J. Wiebe, and R. Wiesendanger, *Science* **320**, 82 (2008).

⁴F. Meier, K. von Bergmann, J. Wiebe, M. Bode, and R. Wiesendanger, *J. Phys. D: Appl. Phys.* **40**, 1306 (2007).

⁵J. Bardeen, *Phys. Rev. Lett.* **6**, 57 (1961).

⁶J. Tersoff and D. R. Hamann, *Phys. Rev. Lett.* **50**, 1998 (1983); *Phys. Rev. B* **31**, 805 (1985).

⁷O. O. Brovko, V. S. Stepanyuk, W. Hergert, and P. Bruno, *Phys. Rev. B* **79**, 245417 (2009).

⁸K. Tao, V. S. Stepanyuk, W. Hergert, I. Rungger, S. Sanvito, and P. Bruno, *Phys. Rev. Lett.* **103**, 057202 (2009).

⁹X.-D. Ma, D. I. Bazhanov, O. Fruchart, F. Yildiz, T. Yokoyama, M. Przybylski, V. S. Stepanyuk, W. Hergert, and J. Kirschner, *Phys. Rev. Lett.* **102**, 205503 (2009).

¹⁰M. Bode, S. Heinze, A. Kubetzka, O. Pietzsch, X. Nie, G. Bihl-

mayer, S. Blügel, and R. Wiesendanger, *Phys. Rev. Lett.* **89**, 237205 (2002).

¹¹C. Li, A. J. Freeman, H. J. F. Jansen, and C. L. Fu, *Phys. Rev. B* **42**, 5433 (1990).

¹²P. Weinberger, *Phys. Rev. B* **80**, 060403(R) (2009).

¹³J. Zabloudil, R. Hammerling, L. Szunyogh, and P. Weinberger, *Electron Scattering in Solid Matter* (Springer, Berlin, New York, 2004).

¹⁴P. Weinberger, *Magnetic Anisotropies in Nanstructured Matter* (CRC, Boca Raton, London, New York, 2008).

¹⁵Only in the absence of time-reversal symmetry chirality effects can occur.

¹⁶Within a linear-response description for the current as used in the Kubo-Greenwood equation such an assumption can always be made.

¹⁷It should be noted that only in the so-called two-current model, namely, in a nonrelativistic version of the Kubo equation, the current $\vec{j} = \sum_s \vec{j}_s$, $\vec{j}_s = \sigma_s \vec{E}_s$, can be associated with a spin index s , provided of course that the (classical) electric field also carries an (artificial) spin index. For further aspects, see, e.g., in *Spin*

- Dependent Transport in Magnetic Nanostructures*, edited by S. Maekawa and T. Shinjo (CRC, Boca Raton, London, New York, 2002), Chap. 2.
- ¹⁸P. Weinberger, A. Vernes, B. L. Gyorffy, and L. Szunyogh, *Phys. Rev. B* **70**, 094401 (2004); A. Vernes, P. Weinberger, and L. Szunyogh, *ibid.* **72**, 012401 (2005).
- ¹⁹S. H. Vosko, L. Wilk, and M. Nusair, *Can. J. Phys.* **58**, 1200 (1980).
- ²⁰L. Szunyogh, B. Újfalussy, C. Blaas, U. Pustogowa, C. Sommers, and P. Weinberger, *Phys. Rev. B* **56**, 14036 (1997).
- ²¹P. Weinberger, *Phys. Rev. B* **75**, 064405 (2007).
- ²²R. Hammerling, C. Uiberacker, J. Zabloudil, P. Weinberger, L. Szunyogh, and J. Kirschner, *Phys. Rev. B* **66**, 052402 (2002).
- ²³D. Sander (private communication).
- ²⁴A. Vernes, B. L. Gyorffy, and P. Weinberger, *Phys. Rev. B* **76**, 012408 (2007).
- ²⁵B. Lazarovits, L. Szunyogh, and P. Weinberger, *Phys. Rev. B* **65**, 104441 (2002).
- ²⁶C. Etz, B. Lazarovits, J. Zabloudil, R. Hammerling, B. Újfalussy, L. Szunyogh, G. M. Stocks, and P. Weinberger, *Phys. Rev. B* **75**, 245432 (2007).
- ²⁷K. Palotás, B. Lazarovits, L. Szunyogh, and P. Weinberger, *Phys. Rev. B* **70**, 134421 (2004).
- ²⁸M. Bode, M. Heide, K. von Bergmann, P. Ferriani, S. Heinze, G. Bihlmayer, A. Kubetzka, O. Pietzsch, S. Blügel, and R. Wiesendanger, *Nature (London)* **447**, 190 (2007).
- ²⁹P. Weinberger, *Phys. Rev. Lett.* **100**, 017201 (2008); *Phys. Rev. B* **78**, 172404 (2008).